Direct acceleration of solid-density plasma bunch by ultraintense laser

Wei Yu,[1,2] H. Xu,[2] F. He,[2] M. Y. Yu,[3] S. Ishiguro,[1] J. Zhang,[4] and A. Y. Wong[5]
[1]*National Institute for Fusion Science, 322-6 Oroshi-cho, Toki-shi 509-5292, Japan*
[2]*State Key Laboratory of High Field Laser Physics, Shanghai Institute of Optics and Fine Mechanics, P. O. Box 800-211, Shanghai 201800, China*
[3]*Institut für Theoretische Physik I, Ruhr-Universität Bochum, D-44780 Bochum, Germany*
[4]*Institute of Physics, Chinese Academy of Sciences, Beijing 100080, China*
[5]*Department of Physics, University of California, Los Angeles, California 90024, USA*
(Received 21 January 2005; published 3 October 2005)

The interaction of a petawatt laser with a small solid-density plasma bunch is studied by particle-in-cell simulation. It is shown that when irradiated by a laser of intensity $>10^{21}$ W/cm^2, a dense plasma bunch of micrometer size can be efficiently accelerated. The kinetic energy of the ions in the high-density region of the plasma bunch can exceed ten MeV at a density in the 10^{23}-cm^{-3} level. Having a flux density orders of magnitude higher than that of the traditional charged-particle pulses, the laser-accelerated plasma bunch can have a wide range of applications. In particular, such a dense energetic plasma bunch impinging on the compressed fuel in inertial fusion can significantly enhance the nuclear-reaction cross section and is thus a promising alternative for fast ignition.

DOI: 10.1103/PhysRevE.72.046401 PACS number(s): 52.38.Kd, 52.57.Fg, 52.65.Rr

INTRODUCTION

Schemes for fast ignition (FI) in inertial confinement fusion (ICF) have recently been extensively studied [1,2]. In FI, the compressed fuel is ignited by a separate pulse of high-intensity laser or charged-particle pulse. It has been proposed [2] that a laser-accelerated proton pulse at the MeV or tens of MeV level can be used for FI since the ions have excellent coupling efficiency at the end (Bragg peak) of their range and can thus deliver their energy to a well-defined volume inside the pre-compressed fuel. This scheme for FI makes use the fact that when a thin foil is irradiated by a petawatt (PW) laser, the relativistic electrons generated in the laser-plasma interaction can easily propagate through the foil and form an electron sheath or cloud on its backside, the resulting electrostatic space-charge field then pulls out and accelerates the protons on the back foil surface to several MeV [4–7]. However, the proton density (usually <0.001 the critical density) is too low for FI. To achieve the necessary beam brightness, Roth *et al.* [2] proposed to use multiple petawatt laser beams and a curved foil in order to ballistically focus the laser-accelerated protons to a small spot in the fuel. Another obstacle for FI may come from space-charge driven defocusing, or Coulomb explosion, of the extremely high proton current. Roth *et al.* [2] suggested that space-charge neutralization by the electrons in the sheath can to some extent prevent the defocusing effect and enable the charged particles be accelerated as a *plasma*.

Recently, Esirkepov *et al.* [3] studied a different regime of proton acceleration from laser-irradiated foil. In their numerical simulation, a thin foil at 50 times the critical density (n_c) is irradiated by a laser with power up to 380 PW. A small (of the laser spot size) part of the foil plasma at the laser focus is strongly pushed forward, while the rest of the plasma remains stationary or moves slowly. Due to the extremely high radiation pressure, a GeV proton bunch of $3n_c$ is thereby generated and moves along the laser propagation axis. As in normal laser-foil interactions [4–7], strong charge separation, with spatial scale comparable to the foil thickness, is induced by the ultraintense laser [3].

In order to avoid the stationary and slowly moving regions of the larger foils [3] as well as charge-separation effects, we propose the use of a small target with radius less than the laser spot size. It is shown by particle-in-cell (PIC) simulation that when such a small target is irradiated by a petawatt laser pulse which acts like a piston [8,9], the resulting pellet plasma is strongly accelerated forward by the laser ponderomotive force and its backside strongly compressed into a high-density shock layer. Simultaneously, the oversized rim of the laser spot wraps around the pellet and acts like a guide, providing it with radial (ponderomotive) confinement as well as directional stability at the critical initial moment of laser impact. The shock layer is unstable and rapidly breaks up into small high-density regions that turbulently reorganize or dissipate until a single high-density region appears. In the process, the electrons in the shock layer are turbulently heated, and the plasma bunch then expands asymmetrically in a rocketlike manner. Even after the laser pulse is reflected, the remaining high-density region continues to accelerated forward within the rapidly moving ($0.1c$ or higher) plasma bunch, accompanied by gradual reduction of its density. Furthermore, except in the early stage of the interaction, the evolution is apparently ambipolar everywhere in the plasma bunch. That is, charge separation and hence Coulomb explosion do not occur. The kinetic energy of the ions in the bunch's densest region, or hard spot, can exceed ten MeV at a density of $\sim 10^{23}$ cm^{-3}. The corresponding particle flux is thus orders of magnitude higher than that of the *charged-particle* pulses accelerated by petawatt lasers [2–10].

 ©2005 The American Physical Society

A SIMPLE MODEL

It is instructive to start with a simple mechanical model, in which a laser pulse with total energy $N_i\hbar\omega_i$ acts on a nondeformable *solid pellet* of mass M, where N_i is the total photon number in the laser pulse and $\hbar\omega_i$ the incident photon energy. The pellet gains the kinetic energy $(\gamma-1)Mc^2$, and the laser pulse is reflected with the total energy $N_r\hbar\omega_r = RN_i\hbar\omega_i$, where N_r is the number of reflected photons, $\hbar\omega_r$ is the reflected photon energy, and R is the reflection coefficient.

Conservation of momentum and energy gives

$$N_i\hbar\omega_i/c = -N_r\hbar\omega_r/c + Mc\gamma\beta, \tag{1}$$

$$N_i\hbar\omega_i = N_r\hbar\omega_r + Mc^2(\gamma-1), \tag{2}$$

where $\gamma=(1-\beta^2)^{-1/2}$, $\beta=V/c$, and V is the pellet velocity. We then obtain

$$\beta = 2q(q+1)/(2q^2+2q+1), \tag{3}$$

$$R = 1/(2q+1), \tag{4}$$

where $q=N_i\hbar\omega_i/Mc^2$ is the ratio between the incident laser energy and the rest energy of the pellet. Equations (3) and (4) give β and R in terms of the initial parameter q.

For low-energy laser-target interaction, q is very close to zero, and we obtain $\beta=0$ and $R=1$. That is, the laser is reflected and the interaction does not cause pellet motion. However, for the ultraintense laser and small pellet under consideration, the ratio q can be appreciable. In this case, the reflection is not total. The pellet gains momentum and energy from the laser pulse, and is accelerated forward. For example, for $q=0.15$ we have $\beta=0.25$ and $R=0.77$, and for $q=0.3$ we have $\beta=0.49$ and $R=0.62$.

This simple model assumes that the pellet remains a solid during the interaction. In the real situation, the ionized pellet would behave like a dense plasma bunch. To investigate the plasma dynamics involved, we have performed two-dimensional (2D) PIC simulations of the laser-pellet interaction and the subsequent motion of the plasma bunch. In the simulations, the simple model is used as a guide in the choice of the relevant parameter ranges.

PIC SIMULATION

We have performed 2D3V (two dimensional in space and three dimensional in velocity) PIC simulations to study the interaction of a linearly polarized Gaussian laser pulse with a small pellet plasma. The laser wavelength is $\lambda_0=1\mu$m, with full width at half maximum (FWHM) $D=10\lambda_0$, spot radius $w=5\lambda_0$, and strength parameter $a=70$. Thus we are in the highly relativistic regime, and the laser magnetic force is dominant. The pellet is initially $3\lambda_0$ in width and $1\lambda_0$ in thickness, its density is $n_0=100n_c$, where $n_c=10^{21}$ cm^{-3} is the critical density. The corresponding laser intensity is 6.8×10^{21} W/cm^2 and the power is 2.7 PW. This choice of the laser and plasma parameters has been guided by the analytical model in the previous section. In particular, these parameters correspond to $q=0.15$, which ensures that the pellet will be set into motion appropriately.

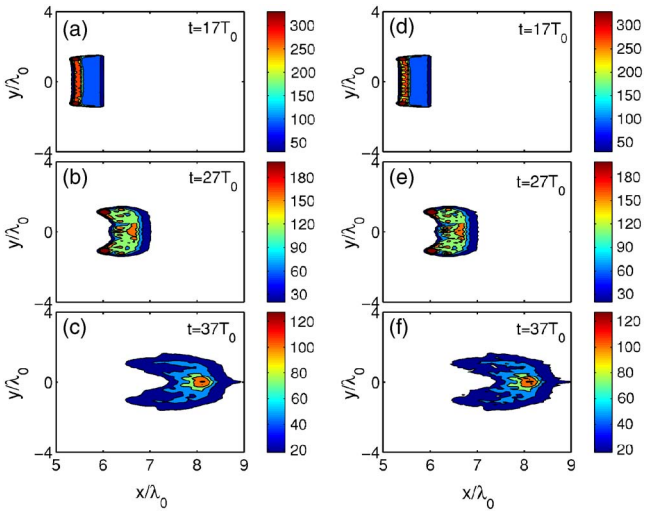

FIG. 1. (Color online) The 2D distribution of ion density (left) and electron density (right) at $t=17T_0$, $27T_0$, and $37T_0$, respectively. Here T_0 is the laser period, $D=10\lambda_0$ its FWHM pulse width, $w=5\lambda_0$ its spot radius, and $a=70$ its strength parameter. The initial pellet density is $n=100n_c$, its width is $3\lambda_0$, and its thickness is $1\lambda_0$ (located at $5<x/\lambda_0<6$). The bars are for the ion and electron densities normalized by n_c.

In the simulation, the computation box is $30\lambda_0\times20\lambda_0$, the spatial resolution is 40 cells per wavelength, and each cell contains 500 ions and 500 electrons. The electron-ion mass ratio is 1/1832, the initial temperatures of the Maxwellian electrons and ions are 1 KeV, and the time step in the simulation is $0.01T_0$, where T_0 is the laser period. The boundary conditions are: periodic in y and absorbing in x.

Figure 1 shows the 2D distributions of the ion (left panel) and electron (right panel) densities at $t=17T_0$, $27T_0$, and $37T_0$. At $t=0$, the peak of the laser pulse is at $x=-D=-10\lambda_0$ and the pellet at $5\lambda_0<x<6\lambda_0$. Figure 2 shows the

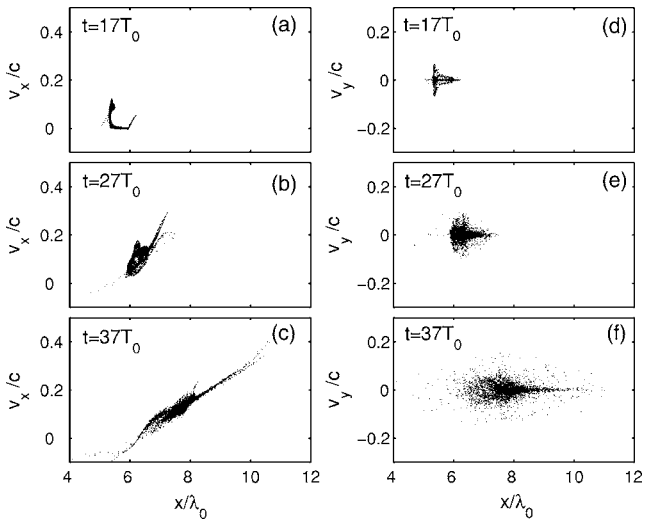

FIG. 2. Phase plots with longitudinal ion velocity V_x/c (left) and traverse ion velocity V_y/c (right) at $t=17T_0$, $27T_0$, and $37T_0$, respectively. The laser and pellet parameters are the same as in Fig. 1.

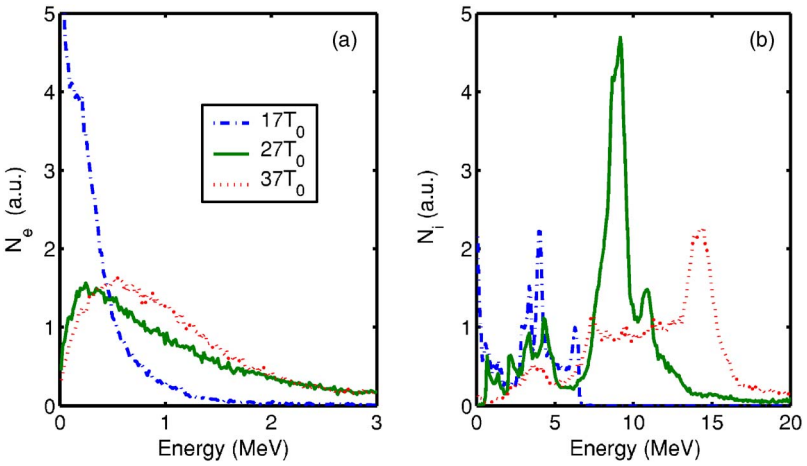

FIG. 3. (Color online) The energy distribution functions of electron (a) and ion (b) along the axis of laser propagation at $t=17T_0$ (dash-dot curves), $27T_0$ (solid curves), and $37T_0$ (dotted curves), respectively. The parameters are the same as in Fig. 1. The energy distribution function is in arbitrary units (a.u.).

corresponding axial and transverse ion velocities V_x (left panel) and V_y (right panel), respectively. From Figs. 1 and 2, one can clearly see that the pellet plasma is accelerated as well as strongly compressed on the backside by the laser. At $t=37T_0$, the plasma ions in the high-density hard spot within the bunch achieve $0.18c$. The corresponding ion kinetic energy is 15 MeV and the plasma density is $\sim 10^{23}$ cm^{-3}.

Comparing the left and right panels in Fig. 1, we see that except in the highly compressed shock layer at $17T_0$, there is no observable charge separation in the plasma bunch. That is, the particles in the bunch indeed behave like a plasma, and space-charge defocusing or Coulomb explosion, common to intense charged-particle beams, is avoided. Although at the initial impact the laser ponderomotive force acts only on the plasma electrons, the resulting electron displacement creates an electrostatic space-charge field which under the present target conditions rapidly restores charge neutrality by accelerating the ions and decelerating the electrons. In particular, the high pellet density helps in suppressing the charge separation. If the pellet density were reduced to, say $n_0=10n_c$, charge separation would be clearly visible. However, even in that case structures like electron sheath and ion layer, common in existing laser-foil interactions, do not appear in the present target configuration.

In addition to laser-driven acceleration, the plasma bunch is compressed and turbulently heated by the laser. That is, the laser energy is converted not only into directed kinetic energy, but also into random internal energy, of the bunch plasma, or more precisely, into the electron thermal energy. Figure 3 shows the energy distributions of (a) electrons and (b) ions along the direction of laser propagation at different times. In the following we shall discuss the different processes in more detail.

ACCELERATION OF THE HARD SPOT

We now discuss in more detail the acceleration of the ions. Roughly, three stages can be identified in the evolution of the plasma pellet.

First, as can be seen in Figs. 1–3 at $t=17T_0$ (recall that initially the pellet plasma is located at $5<x/\lambda_0<6$), the rear (laser) side of the pellet is strongly compressed by the laser, while the pellet remains at rest. The peak density in the compressed region is several times that of the initial pellet density. Since the spotsize is larger than the pellet, the noninteracting part of the laser field actually wraps around the pellet. The resulting radial ponderomotive force at the vacuum-plasma boundary provides radial compression and confinement as well as directional stability of the pellet. The highly compressed region behaves like an unstable shock layer. We can also see two very high-density regions at the back corners of the pellet. These can be attributed to the very strong ponderomotive force there, since the (larger in cross section) laser wraps around the sharp pellet corners.

In the next stage, as shown in Figs. 1–3 at $t=27T_0$, although the tail of the $10T_0$-long laser pulse is still interacting with the plasma bunch, the main part of the laser has reflected and its noninteracting rim has overtaken the pellet. We see that a fast-evolving instability has turbulently broken up the highly compressed shock layer appearing at $17T_0$ into small fragments, together with a larger one with high density at the center. The latter hard spot moves forward within the accelerating and deforming plasma bunch. One can also see that at this stage the two high-density spots at the rear corners of the bunch have slightly increase in size. But they remain relatively stable and are less accelerated.

In the third stage, as shown in Figs. 1–3 at $t=37T_0$, the laser-plasma interaction has ended. We can see that the smaller high-density fragments have either further disintegrated or merged with the center one. The latter has increased in size and density, and it is still accelerating forward. The plasma bunch as a whole is also still deforming. In particular, in the time between $27T_0$ and $37T_0$, the two small back-corner high-density hard spots have disappeared, and a long double tail has formed.

The remaining fairly large hard spot keeps moving towards the front of the already fast-moving plasma bunch. This forward motion within the bunch is at the expense of the rest of the plasma. The rocketlike asymmetrical expansion and elongation of the plasma bunch allows the hard spot to continue accelerating even at $t=37T_0$, when there is no more laser action. Furthermore, as mentioned the two very high density regions at the edges of the shock layer at first evolve slowly (between $17T_0$ and $27T_0$), but then very rapidly (note that between $27T_0$ and $37T_0$ these two regions

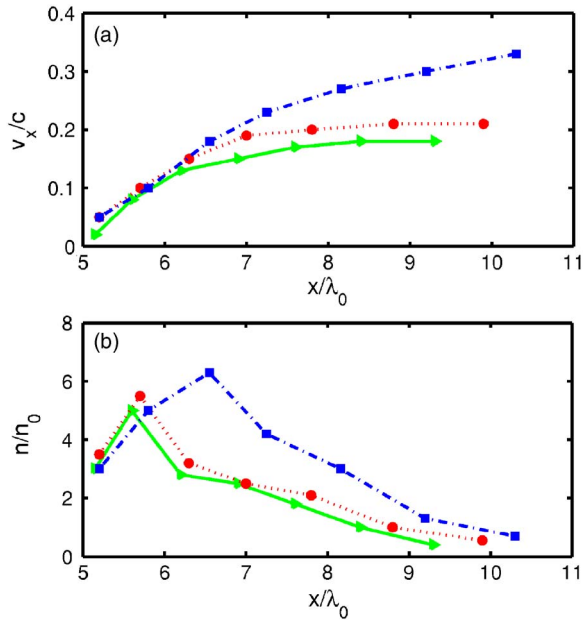

FIG. 4. (Color online) The longitudinal ion velocity V_x/c (a) in the hard spot as function of the position of the hard spot. The dotted curves are for a Gaussian laser pulse of FWHM $D=10\lambda_0$. The parameters are the same as in Fig. 1. The solid curves are for a Lorentzian laser pulse of the same FWHM. The dash-dot curves are for a long ($D=20\lambda_0$) Gaussian pulse.

went from the highest density in the color scale to the lowest density) into a double-tail. The jetlike long tails are formed when the plasma in the two edge hard spots expands in a rocketlike manner, a process which adds to the forward acceleration of the front part of the plasma bunch.

Figure 4, which shows the (ion) speed of the highest density region at the center of the plasma bunch, also demonstrates that the asymmetrical reorganization inside the latter continues at later times. For example, when the hard spot is at $x=8\lambda$, the ion density is close to $2n_0$ and the ion energy close to 15 MeV (or $V_x\sim 0.18c$). In fact, for the short Gaussian laser pulse case, the acceleration is still continuing when the hard spot is at $x=10\lambda$.

HEATING AND EXPANSION

As expected, the turbulent evolution strongly affects the energy distributions of the particles in the bunch. From the electron energy distributions in Fig. 3(a), we find that the mean electron energy increases from 0.4 MeV at $t=17T_0$ to 1.2 MeV at $t=27T_0$, but decreases to 0.8 MeV at $t=37T_0$. The electron energy distribution apparently remains near-Maxwellian at all times. On the other hand, Fig. 3(b) shows that the ions are already highly non-Maxwellian even at $t=17T_0$, and at later times most of them are in the high energy regime, whose mean energy keeps on increasing. It should be pointed out that since the electrons move with the ions, their ordered energy is only 1–10 KeV, and is much smaller than their random energy. On the other hand, the ions have little thermal motion and the ion energy is mainly in the directed motion. Turbulent heating of the electrons also causes the plasma bunch to expand, as indicated by the slow increase of the radial size of the bunch. The evolution of the heated plasma remains apparently ambipolar. In fact, as mentioned, except inside the unstable shock layer at early times, the entire evolution of the plasma bunch appears to be ambipolar in the period under consideration.

Physically, it is clear that after the laser pulse has decoupled there cannot be any acceleration of the bunch as a whole. The acceleration of the hard spot (as shown in Fig. 4 at larger x values) is then purely due to the rocketlike expansion within the bunch, which becomes highly elongated.

As can be seen in Fig. 2(a), even at $17T_0$ fast ions have already appeared in the pellet front, starting with zero velocity at the surface. These may have led to the sharply pointed low-density front in Figs. 1(c) and 1(f). The physics of this phenomenon is not quite clear. For example, it could have been started by the ponderomotive action of the wrap-around laser field during the laser-pellet interaction or by the acceleration of the ions originally residing in the front surface of the pellet by the charge-separation field created by fast electrons, as in normal laser-foil interaction [4–7]. In FI, the very low-density high-energy front can serve as spearhead for the immediately following high-density hard spot.

EFFECT OF PULSE PROFILE

As in other schemes involving laser-foil interaction, the laser pre-pulse can cause undesirable effects, a too strong pre-pulse can blow away or destroy the target before the main pulse arrives. The desired result can also be sensitive to the laser-pulse shape. For the proposed acceleration scheme here, a pulse with modified Gaussian profile having a much steepened front, such as that proposed by Esirkepov *et al.* [3], would be desirable. However, in practice it is difficult to control the exact intensity distribution of the laser pulse.

To examine the effect of the laser pulse shape and length, we have also performed the simulation using Lorentzian and longer Gaussian laser pulses. The Lorentzian pulse has the same FWHM and other parameters as the Gaussian pulse used in obtaining Figs. 1 and 3. In Fig. 4, the solid curves show the ion velocity of the high-density region for the Lorentzian pulse. The dotted curves are for the corresponding Gaussian pulse. The dash-dot curves are for a longer ($D=20\lambda_0$) Gaussian pulse.

We see that the compression and acceleration of the plasma bunch is not much affected by the laser-pulse profile. In particular, the laser profile almost does not affect the ion velocity and density of the hard spot, which is most relevant for FI, in the bunch. Clearly, the pulse profile also does not affect the physics involved.

By increasing the incident laser energy, the value of q is increased, and the plasma bunch should then move faster. This can be seen in Fig. 4 by comparing the curves for the long Gaussian laser pulse having FWHM $D=20\lambda_0$ (corresponding to $q=0.3$) with that of the short pulse. The axial ion velocity V_x corresponding the maximum axial ion density for this case are given by the dash-dot curves in Figs. 4(a) and 4(b), respectively. Initially, the plasma bunch is pushed by

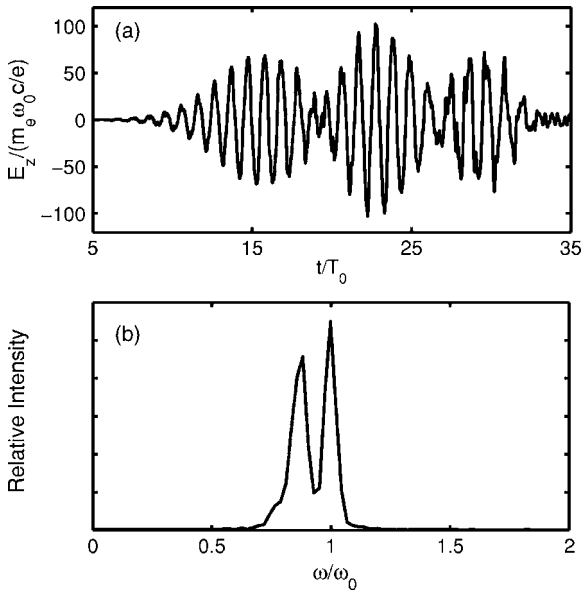

FIG. 5. The time evolution (a) and frequency spectrum (b) of the laser electric field E_y at $x=1\lambda_0$. The spectrum is in arbitrary units. The parameters are the same as in Fig. 1.

laser ponderomotive force in the same manner as in the short-pulse case. But now the direct acceleration and compression by the long-pulse laser last for a longer time, so that more laser energy is deposited to the plasma pellet. As a result, the hard spot in the bunch reaches a density of $6n_0$ and the ions there achieve an axial velocity of $0.2c$. That is, the additional energy input from the longer laser pulse increases the speed as well as the density of the hard spot. It also results in an increase of the duration of asymmetric acceleration of the hard spot after the laser has reflected. The simulation shows that when the maximum density of the expanding plasma bunch eventually reduces to its initial value $n_0(=10^{23}\ \mathrm{cm}^{-3})$, the plasma ions there are accelerated to $0.3c$, with the corresponding kinetic energy reaching 45 MeV.

REFLECTED PULSE

Valuable information can be obtained by analyzing the reflected laser pulse. Figure 5(a) shows the time evolution of the laser field at $x=1\lambda_0$. The laser and plasma parameters are the same as in Fig. 1. Figure 5(b) shows the frequency spectrum. The larger peak in Fig. 5(b) at $\omega/\omega_i=1$ corresponds to the incident, and the smaller peak to the reflected, laser pulse.

Since the plasma bunch is moving forward during the reflection, the redshift in the reflected light is expected. In Fig. 4(b) the reflected-light frequency peaks at $\omega/\omega_i=0.81$. From the relation

$$\omega_r/\omega_i = (1-\beta)/(1+\beta), \tag{5}$$

between the frequencies of the incident and reflected light for a perfect moving reflector, one obtains approximately $0.11c$ for the average velocity of the target during the interaction. This value agrees well with that from simulation (Figs. 1 and 4). However, from Fig. 5(a), we find that the reflection coefficient at the propagation axis is $R\sim 0.33$, which is much smaller than that $(R\sim 0.77)$ from the solid-target model. This fairly large difference demonstrates that plasma effects can greatly enhance the absorption of laser energy by the dense target. As discussed earlier, a significant amount of the absorbed energy is spent in accelerating the plasma bunch as well as the high-density hard spot inside it.

CONCLUSION

We have shown that irradiance of a small solid-density plasma pellet by an ultraintense laser with spot size larger than the pellet cross section can result in an energetic plasma bunch of high density. The acceleration involves direct ponderomotive acceleration as well as subsequent rocketlike asymmetric plasma expansion. In a sense, the ultraintense laser behaves like a piston: it pushes forward the plasma bunch and compresses it from the rear to form a high-density shock layer inside the bunch. The absorbed laser energy is converted into plasma kinetic and internal energies. The shock layer is highly unstable and the instability involved is Weibel-like [11–13]. While still under laser compression, the former breaks up into small high-density regions that then dissipate or reorganize. As a result of turbulent evolution the plasma electrons are heated anisotropically. After the laser is reflected, the nonuniform plasma bunch continue to expand asymmetrically. A single high-density region (hard spot) remains (for example, at $37T_0$) and it continues to move forward within the bunch at the expense of the backside particles that form a long tail. Furthermore, we have shown that the simple solid-target model can well predict the speed of the accelerated plasma bunch. Clearly it cannot predict the subsequent asymmetrical rocketlike acceleration of the hard spot inside the latter. It should be emphasized that at present the physical details of these rather complex turbulent processes are still not understood and further investigations are needed.

The particle flux provided by such a laser-accelerated plasma scheme is several orders of magnitude higher than that of the traditional charged-particle pulses. The present plasma acceleration scheme can have a wide range of applications. In particular, the charge-neutral superdense energetic plasma bunch is useful for FI in ICF schemes since it can be easily transported to the compressed fuel. It can also greatly enhance the cross section of the nuclear reactions because of the high flux density. Our results also suggest that one can model in the laboratory strong-field astrophysical phenomena in intense shock layers [13] by using short-pulse lasers.

ACKNOWLEDGMENTS

This work was supported by the National High-Tech ICF Committee of China, National Natural Sciences Foundation of China (Project Nos. 10335020/A0506 and 10474081), and the Max Planck Society-Chinese Academy of Sciences Exchange Program.

[1] M. Tabak *et al.* Phys. Plasmas **1**, 1626 (1994).
[2] M. Roth *et al.*, Phys. Rev. Lett. **86**, 436 (2001).
[3] T. Esirkepov *et al.*, Phys. Rev. Lett. **92**, 175003 (2004).
[4] S. Hatchett *et al.*, Phys. Plasmas **7**, 2076 (2000).
[5] R. A. Snavely *et al.*, Phys. Rev. Lett. **85**, 2945 (2000).
[6] M. Zepf *et al.*, Phys. Rev. Lett. **90**, 064801 (2003).
[7] I. Spencer *et al.*, Phys. Rev. E **67**, 046402 (2003).
[8] W. Yu, M. Y. Yu, J. Zhang, and Z. Xu, Phys. Rev. E **58**, 6553 (1998).
[9] W. Yu *et al.*, Phys. Rev. Lett. **85**, 570 (2000).
[10] S. V. Bulanov *et al.* Phys. Plasmas **12**, 073103 (2005).
[11] E. S. Weibel, Phys. Rev. Lett. **2**, 83 (1959).
[12] Y. Sentoku *et al.*, Phys. Rev. E **65**, 046408 (2002), and references therein.
[13] K.-I. Nishikawa, P. Hardee, G. Richardson, and R. Preece, Astrophys. J. **595**, 555 (2003), and references therein.